Control Design and Voltage Stability Analysis of a Droop-Controlled Electrical Power System for More Electric Aircraft

***Abstract*-- This paper focuses on the analysis of a single DC bus multi-generator Electrical Power System (EPS) for future More Electric Aircrafts (MEA). Within such a single bus paradigm, the paper proposes a detailed control design procedure and provides a stability analysis based on the derivation of the output impedance of the source subsystem and input impedance of the load subsystem, including control dynamics. The single bus characteristic is analyzed and the stability properties of the EPS are investigated when supplying constant power loads. In addition, the paper highlights the impact on stability of the number of parallel sources and of the power sharing ratio. The theoretical analysis is instrumental in designing an optimally stable single DC bus EPS. The key findings are validated by experimental results.**

***Index Terms*-- More Electric Aircraft, droop control, single bus, DC power system, multiple source, constant power load, voltage stability.**

I. Introduction

THE more-electric aircraft (MEA) concept is one of the major trends in modern aerospace engineering aiming for reduction of the overall aircraft weight, operation cost and environmental impact. Electrical systems are employed to replace existing hydraulic, pneumatic and mechanical actuators. As a consequence, the onboard installed electrical power increases significantly and this results in challenges in the design of the aircraft electrical power systems (EPS). The tendency is to replace traditional AC distribution with high-voltage DC distribution. This can increase efficiency, reduce weight and remove the need for reactive power compensation devices [1], [2].

In literature, the primary power distribution in aircrafts has been traditionally based on the single-generator-per-bus paradigm with switched distribution providing the connectivity and system integrity. Instead, the proposed "single-bus" concept uses the micro-grid approach in which all the generators and loads are connected to a single distribution bus. This single bus configuration has been widely used in other applications such as residential microgrids [3]. Such a system has the potential to considerably reduce the EPS weight since bus mass is reduced and load and generator fault isolation function can be integrated in power converters; in addition the controlled power sharing between generators has the potential to reduce generator capacity and operate at maximum efficiency levels.

As the parallel operation of multiple generators is a promising solution for the MEA EPS, appropriate power sharing among the different power sources needs to be carefully considered. From the communication point of view, overall control of DC systems can be divided into three categories: distributed control, centralized control and decentralized control [4]. In terms of centralized control, not only a centralized controller is required to send commands to individual modules but also communication links from each parallel module to the centralized controller are needed [5], [6]. Under this circumstance, system failure can occur if communication fails. Distributed control does not need a central controller but communication links among the parallel units are essential [7], [8]. It overcomes the disadvantage of centralized control: single point failure (central controller, communication links), but the performance is still degraded by the communication delays. Alternatively, appropriate power sharing can also be achieved by employing droop control, a decentralized control method which relies on local measurements and control [9], [10]. If the outage of one module occurs, the remaining modules can still contribute to power sharing according to their local droop settings. Thus, the system reliability is increased. Since communication links among the sources and additional centralized controller are not needed, each parallel module can work independently relying on the local measurements and controllers. Therefore, higher system modularity and lower cost can be achieved as well under droop control. Due to the abovementioned advantages, a droop-based solution is an attractive choice for the DC EPS.

Typical loads within the EPS are tightly controlled by power converters and can often behave like constant-power loads (CPLs). The negative input resistance characteristic of the CPL may result in a reduction of the stability margins of the EPS [11], [12]. The candidate EPS control architecture should be carefully examined for stability in order to guarantee safe and predictable EPS operation for a wide range of operation scenarios.

To evaluate voltage stability properties and design a robust EPS, two approaches can be highlighted here. The first option is to consider the stability problem with a general state space model, design the control and evaluate the impact of different parameters by studying the eigenvalues [13]-[15]. A more practical approach is the impedance method, which is based on the ratio of the output impedance of the source subsystem and input impedance of the load system [16]-[19]. Thus, the contribution of each component to the system stability can be assessed in the frequency domain. In addition, the output impedance of the components or subsystems can be reshaped to stabilize the overall power system and the impact of the

connection of new converters can be assessed.

In the specific context of aircraft power systems, so far, several publications have discussed the system stability in MEA EPS. The stability of a switched reluctance motor-based 270V DC EPS has been analyzed in [20]. A permanent magnet synchronous generator (PMSG)-based hybrid AC-DC MEA EPS is investigated in [21], [22] and the influence of parameter variation on system stability is presented. Nevertheless, the published works on the context of MEA EPS are mainly focused on the single source system, droop control is not used and the dynamics of the generator is not taken into account. In [23], stability of a single DC bus MEA EPS with multiple generators is investigated. However, the interaction of the parallel sources including the steady-state power sharing performance is not validated experimentally, and the impact on stability of different operating frequencies of the different sources is not addressed.

In alignment with the single bus concept, this paper presents a design oriented analysis of the single DC bus EPS with multiple sources based on Permanent Magnet Synchronous Generators (PMSGs) for future civil aircrafts.

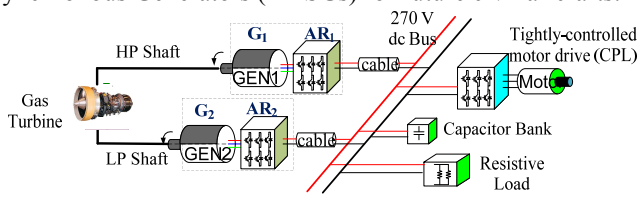

Fig. 1. Configuration of the studied system in the MEA.

As illustrated by Fig. 1, two PMSGs are connected directly to the turbine shafts through active rectifiers (ARs) and can operate in variable speed mode. The two generators take power from the main engine through high pressure (HP) shaft and low pressure (LP) shaft, guaranteeing an efficient exploitation of the power generated by the engine, and operate in parallel to transfer the power to the DC bus. The rated voltage of the main bus in aerospace applications is 270 V, as described in the standard MIL-STD-704F [24]. In this configuration, the two generators can operate at different speeds, typically during climb, cruise, and descent of the aircraft, and as a consequence, the corresponding connected converters operate at different AC input frequencies. As shown later in the analysis, this may lead to voltage instability if the load power is not properly distributed between the two sources. The main contributions of the paper can be highlighted as follows:

(1) Detailed control design for the single bus EPS with multi-source and active/passive loads has been performed.

(2) The steady-state power sharing performance and main bus characteristic are presented.

(3) The interaction between multiple sources (LP/HP generators) has been investigated in terms of voltage stability: the influence of the power sharing ratio between different sources and the increased number of parallel sources on stability are analyzed.

The paper is organized as follows: In Section II, the control strategies for the active rectifier and active load converter are presented and detailed control design procedure is shown. Section III derives the source and load impedances including the control dynamics. The interaction effect between parallel sources on voltage stability as well as on steady-state characteristic are also performed in this Section. Validation of the analysis with experimental results is presented in Section IV.

II. System Modeling and Control Design

The system shown in Fig. 1 can be divided into source and load subsystem with the break point chosen at the DC bus. The definition of the source/load subsystem is based on [25]. The converter which takes part in the bus voltage regulation is defined as the source converter whereas the converter consumes/absorbs the power from the bus is regarded as the load converter. This section will present the detailed control design process for the source and load converter.

Fig. 2 presents the control block diagram of the single PMSG-AR system. By controlling the flux in the *d*-axis and the active power in the *q*-axis, the PMSG can operate in generation mode within the high speed region. Conventional PI controllers are used to deflux the machine (*d*-axis) and control the output DC current (*q*-axis). The stator current references in *d* and *q* axes are obtained from the output of the flux weakening controller and I_{dc} controller respectively. The reference of the AC voltage (v_c) is dependent on the DC voltage. The DC current reference (i_{dc}^*) is determined by the desired droop characteristic. It is worth noting that instead of tightly regulating the DC bus voltage, DC current is the control target in this study in order to regulate the proper injected active power into the DC bus. When using this topology, this control structure should be implemented in all generator-converter modules intended for power flow control.

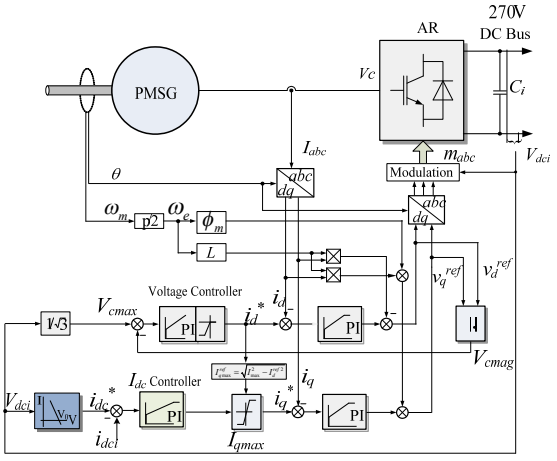

Fig. 2. Control scheme utilized in the single PMSG-AR system.

A. Source Subsystem-Inner Loop

Using the vector control for the PMSG-AR, one can obtain the voltage equations in *dq* frame as

$$\begin{cases} v_d = (R + Ls)i_d - \omega_e L i_q \\ v_q = (R + Ls)i_q + \omega_e L i_d + \omega_e \phi_m \end{cases} \quad (1)$$

where R and L represents the stator resistance and inductance; ω_e is the electrical rotating velocity in rad/s; ϕ_m is the flux linkage of the permanent magnet; i_{dq} is the stator current in d- and q-axis respectively. The control plant of the inner current loop G_{p_idq} can be expressed as

$$G_{P\_idq} = \frac{1}{Ls + R} \tag{2}$$

Assuming the inner current loop is designed to be a first-order system with the central frequency ω_c, the zero of the PI compensator is set to cancel the pole of the plant. The proportional gain k_{pc} and integral gain k_{ic} of the PI controller can be written as follows:

$$k_{pc} = \omega_c L, \quad k_{ic} = \omega_c R \tag{3}$$

B. Source Subsystem-Outer Loop

As shown in Fig. 2, the DC current reference is obtained by the droop characteristic:

$$i_{dci}^* = \frac{v_o - v_{dci}}{k_i} \tag{4}$$

where k_i is the droop coefficient, v_o is the nominal voltage (270 V in this study) and v_{dci} is the local DC output voltage of the converter. Fig. 3 shows the control block diagram of the source converter. As discussed in Section II-A, the inner current loop is simplified by a first-order delay block. In order to simplify the control design, DC terminal voltage V_{dc} is assumed to be constant V_{dco}.

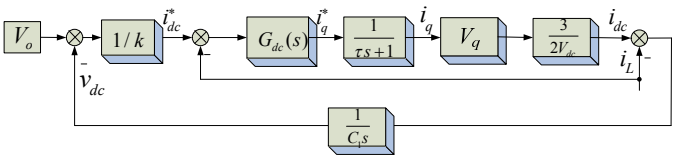

Fig. 3. Control block diagram of the source converter.

As one can see from Fig. 3, the control-to-output (i_{dc} to i_q^*) G_{P_C} can be expressed as below

$$G_{P\_C} = \frac{i_{dc}}{i_q^*} = \frac{3V_{qo}}{2V_{dco}(\tau s + 1)} \tag{5}$$

Given a PI controller of the DC current G_{dc}, the expression for DC current dynamics G_{Dy} can be derived as follows:

$$G_{Dy} = \frac{i_{dc}(s)}{i_{dc}^*(s)} = \frac{G_{P\_C}G_{dc}}{1 + G_{P\_C}G_{dc}} \tag{6}$$

Substituting (5) into (6), the DC current dynamics can be derived as:

$$G_{Dy} = \frac{3V_{qo}(k_{p\_Idc}s + k_{i\_Idc})}{2V_{dco}\tau(s^2 + \frac{2V_{dco} + 3V_{qo}k_{p\_Idc}}{2V_{dco}\tau}s + \frac{3V_{qo}k_{i\_Idc}}{2V_{dco}\tau})} \tag{7}$$

where k_{pdc} and k_{idc} are the proportional gain and integral gain of the I_{dc} controller. Given the damping ratio ξ_{Idc} and natural frequency ω_{Idc}, the following equations can be obtained:

$$2\xi_{Idc}\omega_{Idc} = \frac{2V_{dco} + 3V_{qo}k_{p\_Idc}}{2V_{dco}\tau}, \quad \omega_{Idc}^2 = \frac{3V_{qo}k_{i\_Idc}}{2V_{dco}\tau} \tag{8}$$

From (8), the DC current controller parameters can be derived as follows:

$$k_{p\_Idc} = \frac{2(2\xi_{Idc}\omega_{Idc}\tau - 1)V_{dco}}{3V_{qo}}, \quad k_{i\_Idc} = \frac{2\omega_{Idc}^2\tau V_{dco}}{3V_{qo}} \tag{9}$$

In order to keep a good performance of such a cascaded control loop structure, the bandwidth of the outer loop is chosen as 1/10 of the inner current loop.

C. Load Subsystem

In the load subsystem, apart from the passive loads like resistive loads (RLs), many active loads in EPS such as motor drives and power converters behave as CPLs. In this paper, a buck converter is selected as a representative of CPLs connected to the DC bus, as shown in Fig. 4. The load of the buck converter is a resistor R_{buck} and the buck converter is controlled as a CPL. Different from the conventional control strategies for the buck converter, a current-mode control strategy is presented to achieve the CPL operation, as shown in Fig. 5. V_b represents the bus voltage. As one can see, the inductor current is regulated via a PI controller. The inductor current reference is given according to the load power demand as follows:

$$I_{L_{DC}}^* = \sqrt{\frac{P_{CPL}}{R_{buck}}} \tag{10}$$

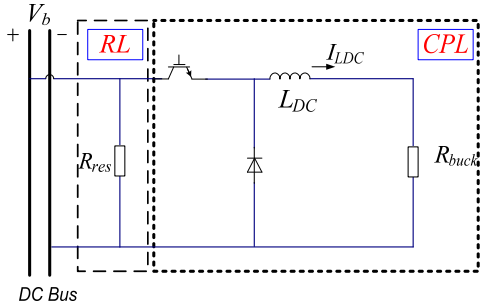

Fig. 4. Power circuit of the load subsystem (resistive load + buck converter).

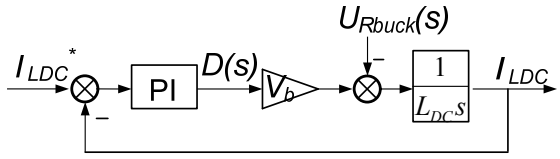

Fig. 5. Control block diagram for the buck converter.

From Fig. 5, the closed loop transfer function of the inductor current I_{LDC} can be expressed as

$$\frac{I_{LDC}(s)}{I_{LDC}^*(s)} = \frac{(k_{pi} + \frac{k_{ii}}{s})(\frac{V_b}{L_{DC}s})}{(k_{pi} + \frac{k_{ii}}{s})(\frac{V_b}{L_{DC}s}) + 1} = \frac{\frac{k_{pi}V_b}{L_{DC}}s + \frac{k_{ii}V_b}{L_{DC}}}{s^2 + \frac{k_{pi}V_b}{L_{DC}}s + \frac{k_{ii}V_b}{L_{DC}}} \tag{11}$$

where k_{pi} and k_{ii} are the proportional gain and integral gain of the PI controller. Given the damping ratio ξ_L and natural

frequency ω_L, the PI control parameters can be derived as follows:

$$k_{pi} = \frac{2\xi_L \omega_L L_{DC}}{V_b},\ k_{ii} = \frac{\omega_L{}^2 L_{DC}}{V_b} \tag{12}$$

To summarize, this section presented the control design for the source converter and load converter, which lays the foundation of the subsequent impedance analysis.

III. Analysis of the Single Bus Multi-Generator System

In the EPS configuration shown in Fig. 1, multiple sources provide electrical power to feed the common DC bus. This section describes the steady-state performance and derives the output impedance of the source subsystem and input impedance of the load subsystem. The voltage stability is then investigated using the impedance-based approach.

A. Steady-State Analysis

The DC-side equivalent circuit of Fig. 1 is presented in Fig. 6. Droop characteristic is implemented by means of an additional current source which is controlled by the local voltage V_{dci}. Since the parasitic capacitance of the cable is much smaller than bus capacitor (C_b) and local capacitor (C_i), it can be included in the converter DC side capacitors and as a consequence, the cable is represented as the *R*-*L* branch.

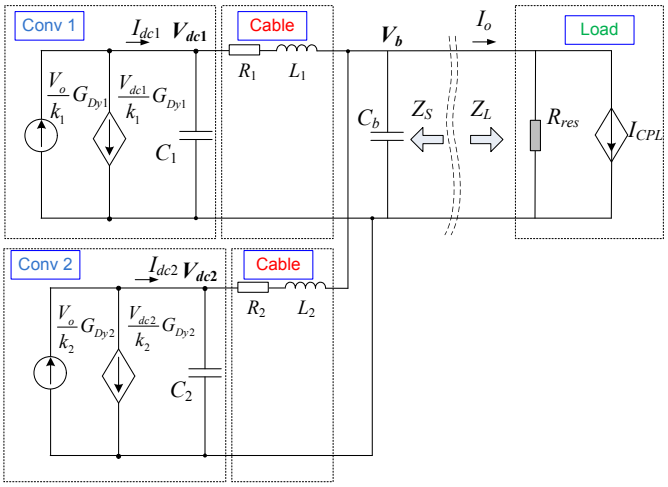

Fig. 6. DC equivalent circuit of the two-source system.

Using droop control, the current sharing ratio among the parallel sources is inversely proportional to the droop gain which can be written as

$$I_{dc1} : I_{dc2} : \ldots : I_{dci} = \frac{1}{k_1} : \frac{1}{k_2} : \ldots : \frac{1}{k_i} \tag{13}$$

Instead of changing the droop slope, the power sharing can be also achieved by adjusting the reference voltage. Under this circumstance, an additional control loop is required to change the reference voltage in order to obtain the desired sharing ratio. In this paper, power sharing control is still implemented by changing the droop gains.

If the system is loaded with CPLs and resistive loads (see Fig. 4), similar to the single source system, the bus voltage V_b and total output current I_o match the following equation:

$$V_b I_o = P_{CPL} + \frac{V_b^2}{R_{res}} \tag{14}$$

Similar to the individual droop line in each parallel source, the steady state V-I characteristic at the DC bus can be expressed as a function of a global equivalent droop coefficient which can be written as below

$$V_b = V_o - I_o k_t \tag{15}$$

Based on (15), the DC bus voltage V_b is determined by the global droop coefficient k_t and load current I_o. The global droop gain can be expressed as a function of individual droop gains [23]:

$$k_t = \frac{1}{\sum_{i=1}^{N} \frac{1}{k_i + R_i}},\quad k_t = \frac{1}{\sum_{i=1}^{N} \frac{1}{k_i}} (if\ k_i \gg R_i) \tag{16}$$

where R_i is the i^{th} branch cable resistance and the droop coefficient is assumed to be much larger than the cable resistance ($k_i >> R_i$).

It can be inferred from (16) that the main bus voltage-current characteristic is still a droop curve which is stiffer than the individual droop characteristic. It indicates that with more number of parallel sources, the voltage deviation at the main bus will be reduced at the same load condition. It also be inferred from (16) that even if the individual droop coefficient settings are different, the bus voltage can be invariant as long as the individual droop coefficients yield the fixed global droop coefficient k_t in (16).

By solving the above equations (14) and (15), the main bus voltage and total current can be derived as follows:

$$V_b = \frac{V_o + \sqrt{V_o^2 - 4k_t P_{CPL}(1+\frac{k_t}{R_{res}})}}{2(1+\frac{k_t}{R_{res}})},\ I_o = \frac{V_o(1+\frac{2k_t}{R_{res}}) - \sqrt{V_o^2 - 4k_t P_{CPL}(1+\frac{k_t}{R_{res}})}}{2k_t(1+\frac{k_t}{R_{res}})} \tag{17}$$

To guarantee existence of a solution for DC voltage and current (17), global droop gain should satisfy

$$k_t < \frac{-R_{res} + \sqrt{R_{res}^2 + \frac{V_o^2}{P_{CPL}} R_{res}}}{2} \tag{18}$$

Physically this can be explained as follows. A larger droop constant will cause larger voltage deviation at the main DC bus and can even result in no intersection point between the source curve and CPL curve. The upper limit shown in (18) is the critical condition to ensure existence of an equilibrium point.

If the global droop gain satisfies the abovementioned requirement, the next step is to decide the injecting current from each parallel source. As one can see from (13), the current sharing ratio is proportional to the inverse of

individual droop gain. Combining (13) and (16), the individual droop gain can be designed as follows:

$$k_i = k_t / n_i, \quad \sum_{i=1}^{N} n_i = 1 \tag{19}$$

where n_i represents the desired current sharing proportion of the i^{th} source and N is the total number of parallel sources.

B. Impedance Analysis

Using the ratio of open-circuit voltage and short-circuit current of the source subsystem, the output impedance of the droop-controlled source subsystem in Fig. 6 can be derived as

$$Z_{Source} = \frac{1}{\sum_{i=1}^{N} \frac{Y_{ib}(C_i s + \frac{G_{Dyi}}{k_i})}{(Y_{ib} + \frac{G_{Dyi}}{k_i} + C_i s)} + C_b s} \tag{20}$$

Where the cable admittance is Y_{ib} and G_{Dyi} is the DC current tracking performance given in (7).

For the load impedance, the input impedance of the buck converter operated with the control strategy discussed above (see Fig. 5) can be derived as:

$$Z_{Load} = -\frac{R_{buck} + L_{DC}s + (k_{pi} + \frac{k_{ii}}{s})V_b}{D_o(D_o + I_{Rbuck\_o}(k_{pi} + \frac{k_{ii}}{s}))} \tag{21}$$

D_o and I_{Rbuck_o} are the operating points for the duty cycle and the output current of the buck converter which can be expresses as below

$$D_o = \frac{\sqrt{P_{CPL} R_{buck}}}{V_b}, \quad I_{Rbuck\_o} = \sqrt{\frac{P_{CPL}}{R_{buck}}} \tag{22}$$

Substituting (22) into (21) yields

$$Z_{Load} = -\frac{V_b^2 L_{DC}}{P_{CPL}(R_{buck} + V_b k_{pi})} \frac{s^2 + \frac{k_{pi}V_b + R_{buck}}{L_{DC}} s + \frac{V_b k_{ii}}{L_{DC}}}{s + \frac{V_b k_{ii}}{R_{buck} + V_b k_{pi}}} \tag{23}$$

After deriving the equivalent source and load impedance, the stability assessment will be evaluated in next subsection.

C. Voltage Stability Analysis

As one can infer from (20) and (21), operating parameters (load power, generator speed) and control parameters (droop gain, control bandwidth), which have a direct/indirect effect on $G_{Dy,}$ will change the source impedance. It is well-known that an increased power absorbed by CPLs will degrade the system stability [21], [22]. The effect of the control parameters was also discussed in [23]. Thus, this paper focuses on the impact of the number of parallel sources and different power sharing ratios between HP and LP sources on the source/load impedance and voltage stability.

(1) Effect of number of parallel sources

If multiple sources work in parallel with the same individual droop coefficient (k_i = 2), the global droop coefficient k_t decreases with the increasing number of parallel sources as expected from (16), as listed in Table I. Fig. 7 shows the Bode plot of the source/load impedance of the parallel sources system. As one can see from Fig. 7(a), the source impedance is reduced with the increased number of parallel sources. Meanwhile, it is observable from Fig. 7(b) that the load impedance magnitude increases with the increasing number of parallel sources. This is because the global droop coefficient decreases with increasing the number of parallel sources, yielding less voltage drop at the main bus under the same load condition. As a consequence, the load impedance at the low frequency region will increase, as indicated from (23). Hence, the system stability is improved if parallel sources are working with the same individual droop coefficient (k_i).

TABLE I
VARYING GLOBAL DROOP GAINS

Number of Sources N	Individual droop k_i	Global droop coefficient (k_t)
1	2	2
2	2	1
3	2	2/3

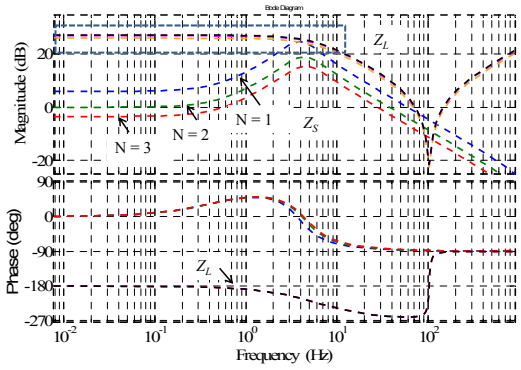

(a)

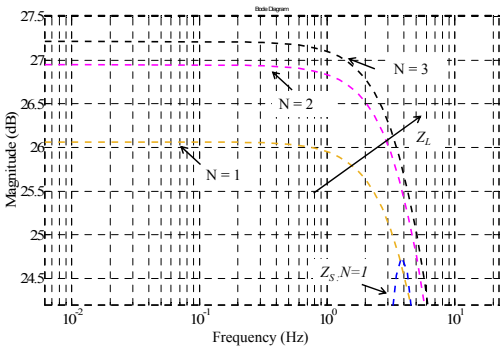

(b)

Fig. 7. Bode plot of source and load impedances in a system with parallel sources. (a) Overview of source and load impedance. (b) Zoomed area for load impedances in (a).

(2) Effect of load sharing ratio

The power sharing among multiple sources can be adjusted by tuning the individual droop gains. This section will investigate the impact of different load sharing ratio on system stability. If the two source is operating at different frequencies (50 Hz for LP source and 400 Hz for HP source), Fig. 8 shows

the equivalent source impedance under different power sharing ratios. It can be observed that the peak magnitude of the overall source impedance decreases if the LP system shares more power. Under the prerequisite that the load power does not exceed the ratings of each generation channel (LP or HP), the Bode plot demonstrates that the parallel system will be more stable if the LP system provides more power to feed the load. This finding would facilitate engineers in designing an appropriate power management scheme that would guarantee voltage stability in a sufficiently wide margin.

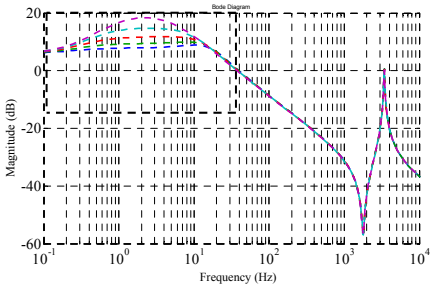

(a)

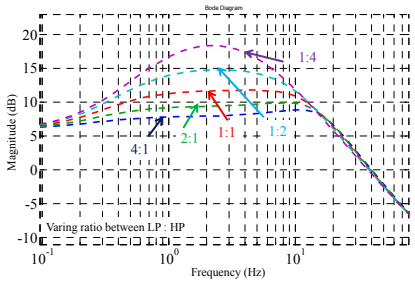

(b)

Fig. 8. Bode plot of source impedance under different load sharing ratio between LP (50 Hz) and HP (400 Hz) channel. (a) Overview. (b) Zoomed area of the dashed rectangular part in (a).

IV. Experimental Validation

A test rig to validate the theoretical analysis developed for the multi-source MEA EPS architectures was designed and built, as shown in Fig. 9. Fig. 10 shows the schematic of the experimental system. The laboratory prototype contains two active front-end converters Conv 1, interfacing the HP generator, and Conv 2, interfacing the LP generator. For the experimental results shown in subsections IV.A and IV.B the two converters are connected to the same programmable AC source (Chroma QuadTech 31120) through two step-down transformers, to emulate two identical synchronous machines, thus focusing on a simplified scenario where HP and LP generators are identical. This choice has been made with the objective of proving the concept of global droop gain and the generic impact of parallel operation on stability. Instead, a different scenario is considered in subsection IV.C, where Conv 1 (HP) and Conv 2 (LP) are connected to two different generators. The control algorithm for both source converters (Conv 1 and 2) is implemented following the same scheme shown in Fig. 2. A DC/DC (buck) converter is tightly controlled as a CPL using the control strategy shown in Fig. 5. To maintain coherence with the theoretical analysis, the experimental system parameters are listed in Table II.

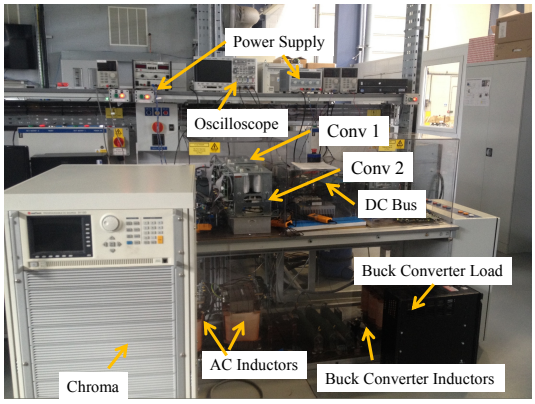

Fig. 9. Test rig.

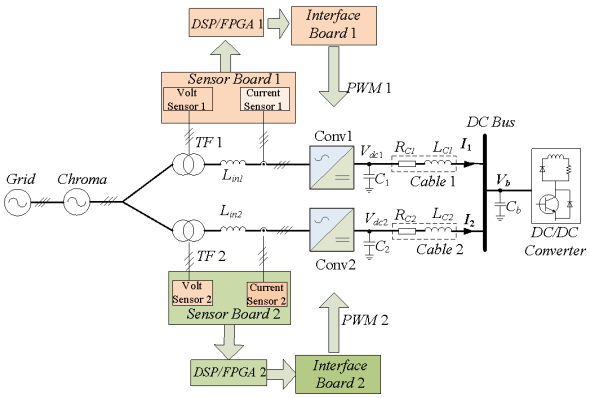

Fig. 10. Schematic of experimental setup used in the results shown in Section IV.A and IV.B.

TABLE II
EXPERIMENTAL SYSTEM PARAMETERS

Category	Parameter	Value
Transformer (TF_1, TF_2)	Transformer	415 V/160 V, Y-y
AC Side Inductor (L_{in1}, L_{in2})	AC side inductor	1.2 mH
c/dc Converter (Buck)	Load	9.7 Ω
	Inductor	1.3 mH
PWM Rectifier (Conv 1, Conv 2)	Switching frequency	12 kHz
Cable (Rc, Lc)	Line resistance	30 mΩ
	Line inductance	5 μH

A. Case 1: Steady-State Investigation

Under a 2.6 kW CPL, the two converters are operating in parallel with the identical individual droop coefficient as listed in Table III. Fig. 11 shows the experimental result of the main DC bus voltage and the injecting DC current from each source. As one can see, the bus voltage decreases as the global droop coefficient k_t increases and the current injected by Conv 1 and 2 are identical. The individual DC currents agree with the expectations in (4) and the main bus V-I characteristic (bus voltage and total load current) is consistent with the discussion in Section III-A.

TABLE III
VARYING GLOBAL DROOP GAINS IN Fig. 11

k_1	k_2	Global droop gain (k_t)
2	2	1
3	3	1.5
4	4	2

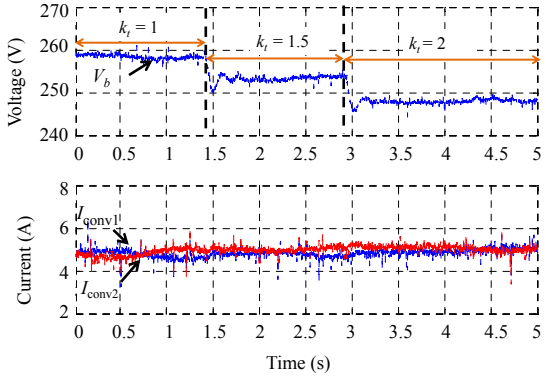

Fig. 11. Experimental result with global droop coefficient variation.

In the next experimental result depicted in Fig. 12, the global droop coefficient k_t is fixed to 1, however the current sharing ratio between two sources is varied, as shown in Table IV. The individual droop coefficients are set according to (19). As one can observe, the steady state bus voltage is not affected by the step changes in the sharing ratio, but the load current provided by Conv 1 and 2 varies according to the set ratio. As before, the results are consistent with the theoretical analysis in Section III-A.

TABLE IV
VARYING POWER SHARING RATIO IN Fig. 12

Power sharing ratio (I_1 : I_2)	k_1	k_2
1:1	1/0.5	1/0.5
3:2	1/0.6	1/0.4
4:1	1/0.8	1/0.2
2:3	1/0.4	1/0.6

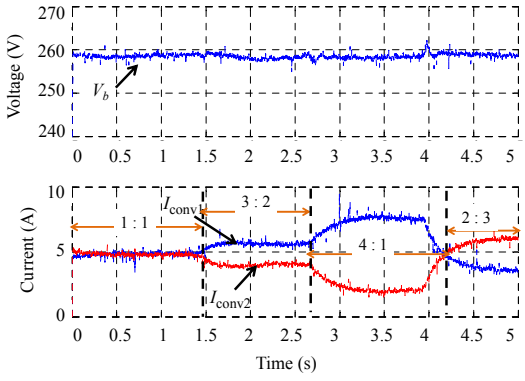

Fig. 12. Experimental result with power sharing ratio variation.

B. Case 2: Stability Analysis-Effect of Parallel Generation

The effect of the number of parallel sources on voltage stability is examined in Case 2. Firstly a single converter (Conv 1) is operated with 200 Hz AC input from Chroma and the droop coefficient k_1 is set to 1. It shows in Fig. 13(a) that the system consisting of a single converter is oscillating at high power load (6 kW). In contrast, Fig. 13(b) shows the experimental result when Conv 2 is connected to a 50 Hz AC source and Conv 1 is disconnected. It can be seen that the system with Conv 2 is still stable when the load power reaches 6 kW.

The effect of parallel operation with the same individual droop gain (k_i = 1) has been also tested. As illustrated in Fig. 10, both converters (Conv 1 and 2) are connected to the with 200 Hz AC supply and Fig. 14 shows the experimental result. At t = 0 s, the load is set at 3kW and only Conv 1 is operating. At t = 1.1 s, Conv 2 is connected and begins to operate in parallel with Conv 1. As a result, the global droop gain reduces and the bus voltage increases. As discussed in Section III-C, the global droop gain reduces with the increased numbers of parallel modules with the same individual droop constant. The overall source impedance reduces and consequently, stability is improved by parallel operation. It can be seen that the two source system is stable below 7kW CPL. This result demonstrates that compared with single source operation, parallel operation with the same individual droop gains significantly improves the system stability which is in accordance with the discussion in Section III-C.

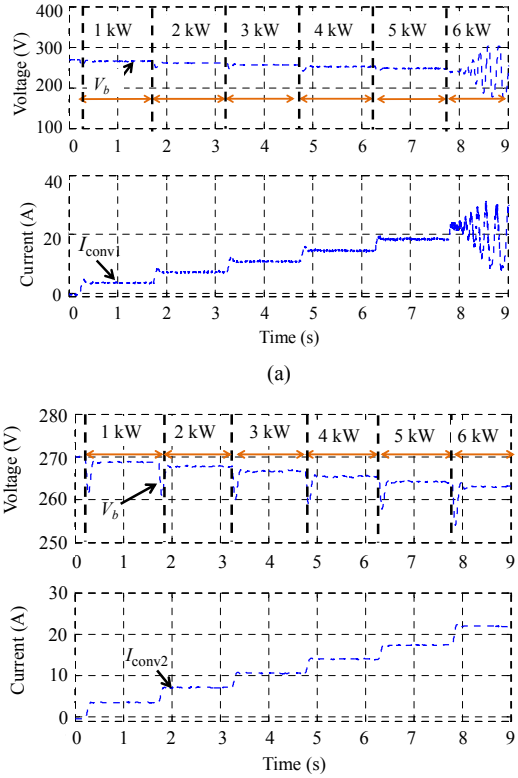

Fig. 13. Experimental results of single source operation: (a) Conv 1 operates at k_1 = 1 and Conv 2 is disconnected. (b) Conv 2 operates at k_2 = 1 and Conv 1 is disconnected.

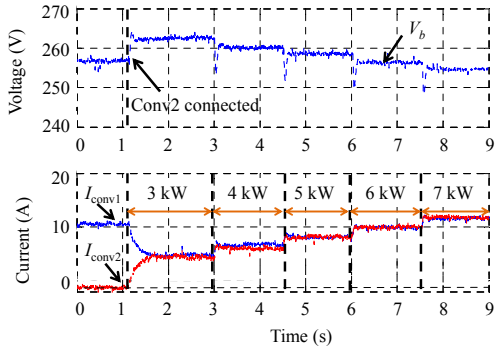

Fig. 14. Experiment result for parallel sources with identical individual droop gains ($k_1 = k_2 = 1$, $k_t = 0.5$).

C. Case 3: Stability Analysis-Effect of Different Power Sharing Ratio

The effect of different power sharing ratio among the parallel sources in Case 3. Different from the previous cases, the Chroma and a Variable Autotransformer are connected to transformer TF1 and TF2 respectively. Under this circumstance, Chroma provides a 200 Hz AC input to Conv 1 and the Variable Autotransformer provides a 50 Hz AC input to Conv 2. Both sources are operated at different frequencies to emulate the HP and LP generators. Global droop gain k_t is fixed at $k_t = 1$. The influence of different power sharing ratio on the system stability has been tested and the result is shown in Fig. 15. When the ratio between HP and LP channel is 3:7, it can be seen from Fig. 15(a) that the system is stable over the load power ranging from 0 to 5 kW. When the power is equally shared between HP and LP channel, oscillation occurs in the presence of 5 kW CPL (see Fig. 15(b)). It can be seen from Fig. 15(c) that instability shows even earlier (4 kW CPL) when the current sharing ratio between HP and LP is set to 7:3. This indicates that the overall system stability will be degraded if the HP generation channel shares more power. Under the ratio HP: LP = 7:3, Fig. 15(d) shows the HP channel AC current (230 V/200 Hz) which is generated from CHROMA and LP channel AC current (230 V/50 Hz) which is generated from the Variable Autotransformer at 1 kW load condition.

The experimental result is consistent with the theoretical analysis in Section III-C, demonstrating that the system is more stable if the LP channel shares more power (see Fig. 8).

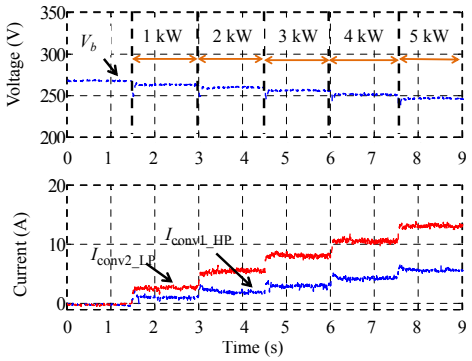

(a)

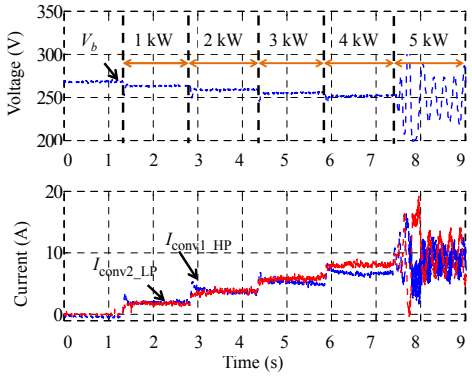

(b)

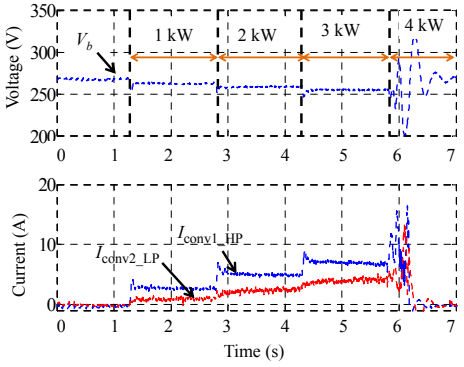

(c)

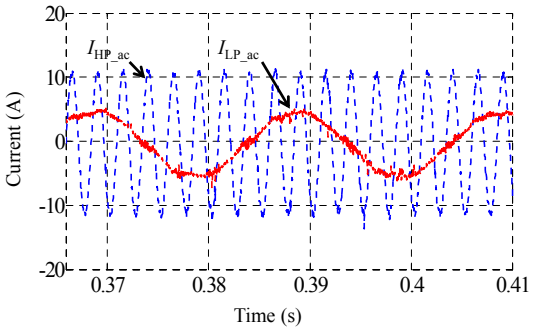

(d)

Fig. 15. Experimental results for different power sharing ratio between the two sources operated at different frequencies. (a) HP: LP = 3:7; (b) HP: LP =1:1; (c) HP: LP = 7:3; (d) AC current at 1 kW CPL in (c).

V. Conclusion

The paper presented a detailed control design and voltage stability analysis for one of the most promising power system architectures for the future MEA: a single bus based multi-source DC EPS. This proposed architecture has the potential to considerably reduce the EPS weight in the MEA. Based on a developed mathematical model of the droop-controlled multi-source system, a detailed control design of the source and load converter is presented. Further, the equivalent source and load impedance have been analytically derived and the stability assessment has been carried out to explore the impact of number of parallel sources and power sharing ratio. The main findings that have been experimentally validated can be highlighted as follows:

(1) Compared to the single source operation, parallel sources operation will reduce the voltage deviation at the DC bus. As a result, the load impedance magnitude increases, the source impedance decreases and consequently the stability is improved.

(2) Different power sharing between HP and LP generators is emulated and it demonstrates that the system is more stable if the LP generator provides more power than the HP generator to feed the bus.

Overall, this paper provides a systematic design and analysis procedure for a future single DC bus EPS.

REFERENCES

[1] D. Salomonsson and A. Sannino, "Low-voltage dc distribution system for commercial power systems with sensitive electronic loads," *IEEE Trans. Power Del.*, vol. 22, no. 3, pp. 1620–1627, Jul. 2007.

[2] P. Wheeler and S. Bozhko, "The more electric aircraft: technology and challenges," *IEEE Electrif. Mag.*, vol. 2, no. 4, pp. 6–12, Dec. 2014.

[3] E. Rodriguez-Diaz, F. Chen, J. C. Vasquez, J. M. Guerrero, R. Burgos, and D. Boroyevich, "Voltage-level selection of future two-Level LVdc distribution grids: A compromise between grid compatibility, safety, and efficiency," *IEEE Electrif. Mag.*, vol. 4, no. 2, pp. 20–28, Jun. 2016.

[4] T. Dragicevic, X. Lu, J. Vasquez, and J. Guerrero, "DC microgrids–Part I: A review of control strategies and stabilization techniques," *IEEE Trans. Power Electron.*, vol. 31, no. 7, pp.4876-4891, Jul. 2016.

[5] S. K. Mazumder, M. Tahir, and K. Acharya, "Master–slave current sharing control of a parallel dc–dc converter system over an RF communication interface," *IEEE Trans. Ind. Electron.*, vol. 55, no. 1, pp. 59–66, Jan. 2008.

[6] J. W. Simpson-Porco, Q. Shafiee, F. Dörfler, J. C. Vasquez, J. M. Guerrero, and F. Bullo, "Secondary frequency and voltage control of islanded microgrids via distributed averaging," *IEEE Trans. Ind. Electron.*, vol. 62, no. 11, pp. 7025–7038, Nov. 2015.

[7] G. Chen, F. L. Lewis, E. N. Feng, and Y. Song, "Distributed optimal active power control of multiple generation systems," *IEEE Trans. Ind. Electron*., vol. 62, no. 11, pp. 7079–7090, Nov. 2015.

[8] L. Meng, T. Dragicevic, J. Roldan-Perez, J. C. Vasquez, and J. M. Guerrero, "Modeling and sensitivity study of consensus algorithm-based distributed hierarchical control for DC microgrids," *IEEE Trans. Smart Grid*, vol. 7, no.3, pp.1504–1515, May 2016.

[9] J. M. Guerrero, M. Chandorkar, T.-L. Lee, and P. C. Loh, "Advanced control architectures for intelligent microgrids–Part I: Decentralized and hierarchical control," *IEEE Trans. Ind. Electron.*, vol. 60, no. 4, pp. 1254–1262, Apr. 2013.

[10] J. M. Guerrero, J. C. Vasquez, J. Matas, L.G. de Vicuña, and M. Castilla, "Hierarchical control of droop-controlled ac and dc microgrids–A general approach toward standardization," *IEEE Trans. Ind. Electron.,* vol. 58, no. 1, pp. 158–172, Jan. 2011.

[11] A. Emadi, A. Khaligh, C. Rivetta, and G. Williamson, "Constant power loads and negative impedance instability in automotive systems: Definition, modeling, stability, and control of power electronic converters and motor drives," *IEEE Trans. Veh. Technol.*, vol. 55, no. 4, pp. 1112–1125, Jul. 2006.

[12] M. Wu and D. D. C. Lu, "A novel stabilization method of LC input filter with constant power loads without load performance compromise in DC microgrids," *IEEE Trans. Ind. Electron.*, vol. 62, no. 7, pp. 4552–4562, Jul. 2015.

[13] A. Singh, A. K. Kaviani, and B. Mirafzal, "On dynamic models and stability analysis of three-phase phasor PWM-based CSI for stand-alone applications," *IEEE Trans. Ind. Electron.*, vol. 62, no. 5, pp. 2698–2707, May 2015.

[14] S. Liu, P. X. Liu, and X. Wang, "Stochastic small-signal stability analysis of grid-connected photovoltaic systems," *IEEE Trans. Ind. Electron.*, vol. 63, no. 2, pp. 1027–1038, Feb. 2016.

[15] L. Wang and M. S. N. Thi, "Stability analysis of four PMSG-based offshore wind farms fed to an SG-based power system through an LCC-HVDC link," *IEEE Trans. Ind. Electron.*, vol. 60, no. 6, pp. 2392–2400, Jun. 2013.

[16] X. Wang, F. Blaabjerg, and W. Wu, "Modeling and analysis of harmonic stability in an AC power-electronics-based power system," *IEEE Trans. Power Electron.*, vol. 29, no. 12, pp. 6421–6432, Dec. 2014.

[17] J. Liu, X. Feng, F. C. Lee, and D. Borojevich, "Stability margin monitoring for DC distributed power systems via perturbation approaches," *IEEE Trans. Power Electron.*, vol. 18, no. 6, pp. 1254–1261, Nov. 2003.

[18] X. Feng, J. Liu, and F.C. Lee, "Impedance specifications for stable dc distributed power systems," *IEEE Trans. Power Electron.*, vol. 17, no. 2, pp. 157–162, Mar. 2002.

[19] J. G. Ciezki and R. W. Ashtion, "Selection and stability issues associated with a navy shipboard DC zonal electric distribution system," *IEEE Trans. Power Del.*, vol. 15, no. 2, pp. 665–669, Apr. 2000.

[20] L. Han, J. Wang, and D. Howe, "Small-signal stability studies of a 270V DC more-electric aircraft power system," in *Proc. Power Electronics Machines and Drives 2006. The 3rd IET International Conference (PEMD)*, Apr. 2006, pp. 197–201.

[21] K-N. Areerak, T. Wu, S. V. Bozhko, G. M. Asher, and D. W. P. Thomas, "Aircraft power system stability study including effect of voltage control and actuators dynamic," *IEEE Trans. Aerosp. Electron. Syst.*, vol. 47, no. 4, pp. 2574–2589, Oct. 2011.

[22] K-N. Areerak, S. V. Bozhko, G. M. Asher, L. De Lillo, and D. W. P. Thomas, "Stability study for a hybrid AC-DC more-electric aircraft power system," *IEEE Trans. Aerosp. Electron. Syst.*, vol. 48, no. 1, pp. 329–347, Jan. 2012.

[23] F. Gao and S. Bozhko, "Modeling and impedance analysis of a single DC bus based multiple-source multiple-load electrical power system," *IEEE Trans. Transp. Electrif.*, vol. 2, no. 3, pp. 335–346, Sep. 2016.

[24] Aircraft Electric Power Characteristics, American Military St. MIL-STD-704F, Mar. 2004.

[25] X. Zhang, X. Ruan, and C. K. Tse, "Impedance-based local stability criterion for DC distributed power systems," *IEEE Trans. Circuits Syst. I, Reg. Papers*, vol. 62, no. 3, pp. 916–925, Mar. 2015.